

51st CIRP Conference on Manufacturing Systems

FEM simulation and acoustic emission based characterization of chip segmentation frequency in machining of Ti-6Al-4V

Frederik Zanger^a, Andreas Kacaras^{a,*}, Matthias Bächle^b, Markus Schwabe^b,
Fernando Puente León^b, Volker Schulze^a

^aInstitute of Production Science, Karlsruhe Institute of Technology, Kaiserstr. 12, 76131 Karlsruhe

^bInstitute of Industrial Information Technology, Karlsruhe Institute of Technology, Hertzstr. 16, 76187 Karlsruhe

* Corresponding author. Tel.: +49-721-608-44015 ; fax: +49-721-608-45004. E-mail address: Andreas.Kacaras@kit.edu

Abstract

FEM chip formation simulations and machining tests of orthogonal cutting were undertaken in order to investigate the influence of cutting speed and tool wear on cutting force, chip segmentation frequency, and residual stress state for Ti-6Al-4V. In addition, acoustic emissions, measured by a piezoelectric sensor adapted to the tool shank, were analyzed to extract chip segmentation frequency in-process using time-frequency representations and periodograms. Results show the capability of robust chip segmentation frequency measuring. The hypothesis of compensating the negative effect of tool wear on the component's residual stress state by means of targeted adjustment of process parameters can be derived.

© 2018 The Authors. Published by Elsevier B.V.

Peer-review under responsibility of the scientific committee of the 51st CIRP Conference on Manufacturing Systems.

Keywords: residual stresses; segmented chip formation; chip segmentation frequency; acoustic emission; machining; tool wear; time-frequency representation; periodogram

1. Introduction

In order to maximize the fatigue strength and thus to provide elongated service life of mechanical components made of Ti-6Al-4V alloy, a defined setting of surface layer states, in particular of the residual stress state, is of elementary importance. Progression in tool wear during machining leading to a change in the thermomechanical load spectrum directly impacts the residual stress state of the machined component [1]. The process-reliable and wear-independent adjustment of the component's residual stress state during the machining of the material Ti-6Al-4V is an objective to strive for in the course of the component's service life. Due to the lack of in-process measurability of the tool wear state and the component's residual stress state during machining, an indirect evaluation based on process characteristics must be used.

During machining Ti-6Al-4V alloy a segmented chip formation can be obtained within the entire reasonable process parameter area [2]. Nguyen et al. [3] investigated the capability of measuring the chip segmentation frequency using a polyvinylidene fluoride (PVDF) thin film piezoelectric dynamic strain sensor in order to characterize the tool wear state in orthogonal cutting of Ti-6Al-4V alloy. It could be demonstrated that the PVDF piezoelectric sensor can be used in-process to characterize the effects of tool wear on the chip segmentation characteristics. It was found that tool wear causes an increase in the chip segmentation frequency and a reduction in the amplitude of chip serration.

On the basis of the already known correlations between tool wear state and the chip segmentation frequency, the possibility of assessing the component's residual stress state by means of the acoustically measured chip segmentation frequency is to be investigated in the context of this work.

Nomenclature

b	width of cut
d	depth
F	energy density of STFT
F_c	cutting force
f	frequency
f_{cs}	chip segmentation frequency
f_s	sample rate
h	cutting depth
P	energy density of periodogram
r_β	cutting edge radius
t	time
t_s	sample time
VB	width of flank wear land
v_c	cutting speed
x	raw AE data
α	clearance angle
β	wedge angle
σ_{RS}^{long}	residual stress in longitudinal direction
σ_{RS}^{trans}	residual stress in transversal direction

2. Process knowledge

In order to determine the possibility of assessing the component's residual stress state by means of the measured chip segmentation frequency the correlation between both values is to be evaluated in the following using chip formation simulation with ABAQUS for the orthogonal cutting of Ti-6Al-4V alloy. The influence of cutting speed and tool wear state on the chip segmentation frequency f_{cs} is studied. The value f_{cs} is evaluated by analyzing the simulated temporal evolution of the cutting force F_c .

2.1. FEM Modelling

A continuous remeshing method for the formation of segmented chips was developed for ABAQUS allowing to avoid intensive element distortions and was demonstrated in [4]. The Johnson-Cook model [5] in combination with the material parameters identified by Recht et al. [6] to describe the workpiece material behavior in the strain hardening area and with the material parameters identified by Sun et al. [7] to describe material failure was used. Friction between the tool and the workpiece was considered using Coulomb's law. The used simulation model has been validated in [4] by comparing cutting forces, temperatures and chip shapes with experimentally achieved results. A K10 series uncoated cutting tool was implemented with geometry parameters shown in Table 1.

Table 1. Geometry parameters of the used cutting insert.

clearance angle α	7°
wedge angle β	77°
cutting edge radius r_β	$30 \mu\text{m}$

2.2. Results and discussion

Figure 1 shows simulated results for the residual stress depth distributions in longitudinal and transversal directions for different cutting speeds v_c and tool wear states VB . Since chip segmentation influences the stress and strain states and thus the component's residual stress states during machining, averaged values of the residual stress states versus different positions behind the tool were stated analogous to Schulze et al. [8].

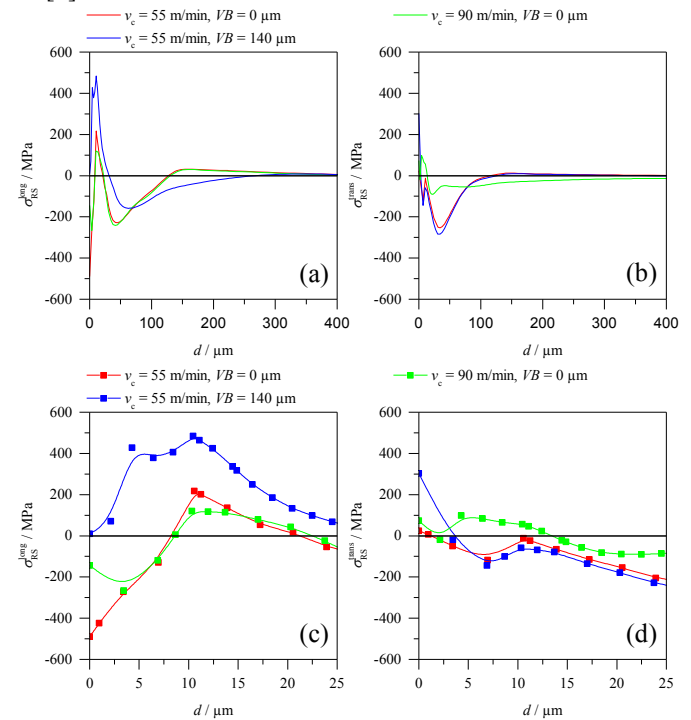


Fig. 1. Simulated residual stress depth distributions in longitudinal (a) and transversal (b) directions for different cutting speeds and tool wear states and corresponding detailed illustration of surface residual stresses (c,d).

On the one hand Figs. 1 (a) and (b) prove the amount of induced compressive residual stresses into the component's surface layer in both directions to be less for increasing tool wear in the depth range up to approximately $70 \mu\text{m}$. Similar results were demonstrated by Chen et al. [9] investigating the effects of tool flank wear and chip formation on residual stress after orthogonal cutting of Ti-6Al-4V alloy by means of experimentally validated FE chip formation simulation. Increasing tool wear led to higher thermal loading in the contact zone between the tool and the workpiece inducing a higher amount of tensile residual stress [9]. On the other hand residual stress depth distributions fitted with a B-spline function in Figs. 1 (c) and (d) show a higher amount of induced surface compressive residual stresses for decreasing cutting speed v_c .

Figure 2 shows simulated results for the temporal evolution of the cutting force F_c for different cutting speeds and tool wear states.

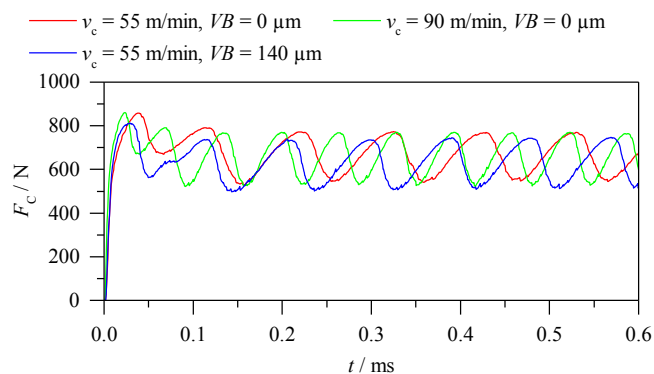


Fig. 2. Simulated temporal evolution of cutting force F_c for different cutting speeds v_c and tool wear states.

During machining of Ti-6Al-4V alloy chip segmentation leads to a periodic temporal force evolution after the occurring impulse caused by the cutting edge entering the material for all simulated configurations. Results show clearly an increasing chip segmentation frequency f_{cs} with growing cutting speed v_c ($\Delta f_{cs, v_c=55/90} \approx 5.6$ kHz). Furthermore, a slight increase of f_{cs} can be stated for a growing tool wear state with $\Delta f_{cs, VB=10/140} \approx 1.4$ kHz. Sun et al. [10] showed that the measured cyclic cutting force during machining of Ti-6Al-4V alloy was a result of chip segmentation and demonstrated the analyzed cyclic force frequency to match the measured chip segmentation frequency.

The chip segmentation has a direct impact on the residual stress depth distribution (see Fig. 1) as well as on the temporal evolution of the cutting force F_c and chip segmentation frequency f_{cs} (see Fig. 2). Therefore, a correlation between cutting speed v_c as process correcting variable, tool wear as process disturbance variable, cutting force F_c , in particular the periodicity f_{cs} of the evolution of the cutting force F_c as process characteristic parameter and the residual stress state as target value can be stated. Consequently the chip segmentation frequency f_{cs} emerges as a process characteristic variable with a high potential for assessing the component's residual stress state during machining.

3. Analysis of acoustic emission signals

Nguyen et al. [3] have shown that in-process analysis of chip segmentation frequency can be done by using a frequency analysis of acoustic emission (AE) signals. They used fast Fourier transform (FFT) for signal analysis and validated their results on the basis of chip segmentations with distinct periodic saw-tooth chip morphology. At lower cutting speeds or feeds, a comparison between f_{cs} obtained by chip analysis and f_{cs} obtained by acoustic emission signals showed higher deviation. One of the reasons identified by Nguyen et al. is the irregularity of periodicity at lower feeds or cutting speeds. This is in compliance with the results from Barry et al. [11], who showed that during machining Ti-6Al-4V, aperiodic saw-tooth chip morphology can occur as well, if process parameters like cutting speed and feed rate are selected below defined thresholds. Then chip segmentation is time-dependent, piecewise periodic with stochastic perturbations or even not measurable in some ranges, because no distinct

periodic part can be identified. The FFT algorithm implies periodic signals and the quality of the results depend on the compliance with the assumption. Therefore, an irregularity in the periodicity or a local variation of f_{cs} distort the chip segmentation frequency obtained by the FFT algorithm. Other authors used time-frequency transformations to process acoustic emission signals such as wavelet packet transform [12], wavelet transform [13] or short-time Fourier transform (STFT) [14].

In the scope of this work, acoustic emission signals are analyzed by STFT in order to measure time-dependent frequencies and cope with piecewise periodic signals.

3.1. Signal acquisition

Orthogonal cutting experiments on Ti-6Al-4V were conducted on a vertical hard broaching machine by Karl-Klink GmbH. The experimental setup is displayed in Fig. 3.

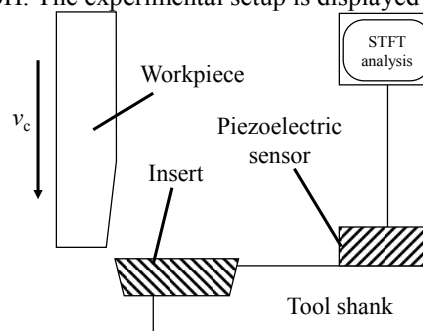


Fig. 3. Schematic view of the experimental setup.

An uncoated carbide insert (P8CC-6090173/WKM CCMW120404) by Walter AG was used for the cutting process. Table 2 shows the corresponding insert geometry parameters.

Table 2. Geometry parameters of the used cutting insert.

clearance angle α	7°
wedge angle β	83°
cutting edge radius r_β	$30 \mu\text{m}$

The workpiece geometry was selected to realize a cutting length of 80 mm and a cutting width of 4 mm. To minimize the impulse caused by the entering of the cutting edge into the material and therefore prevent a fracture of the insert, the workpiece was designed wedge-shaped on the first 30 mm of the cutting length. A piezoelectric sensor was mounted directly onto the tool shank. Acoustic emission measurement during the cutting process was carried out using the AE analyzing device Optimizer4D by QASS GmbH. Thereby, a sample rate of $f_s = 3.125$ MHz was used. The evaluation of the measured raw data was carried out with Matlab software. Table 3 shows the selected process correcting variables for the conducted experiments.

Table 3. Process correcting variables for the orthogonal cutting process.

cutting speed v_c	55 m/min, 90 m/min
cutting width b	4 mm
cutting depth h	$150 \mu\text{m}$

In order to determine the influence of wear on the chip segmentation frequency, new as well as worn inserts were used. The abrasion of the inserts was also carried out by orthogonal cutting. Figure 4 compares the profile sections of the used inserts in initial state and in worn state. The profiles were measured using the contour measuring unit MarSurf XCR20 by Mahr GmbH. The width of flank wear land (VB) was $133\ \mu\text{m}$.

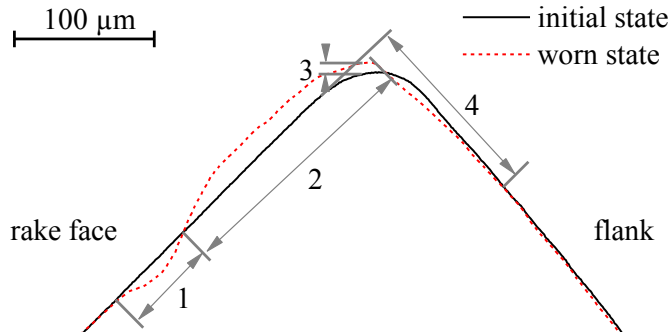


Fig. 4. Comparison of the profile sections of the cutting edges on used cutting inserts. 1) crater wear, 2) built up edge, 3) plastic deformation, 4) flank wear / width of flank wear land VB .

Figure 5 shows light microscopic images of the chips with periodically arranged segmented chips after the orthogonal cutting. The average chip segmentation frequency was calculated with the measured distances between the segments and by neglecting the chip compression. To estimate the influence of the chip compression, the ratio of cutting depth h to the average segmented chip height was calculated and came to values of 1.13 – 1.26.

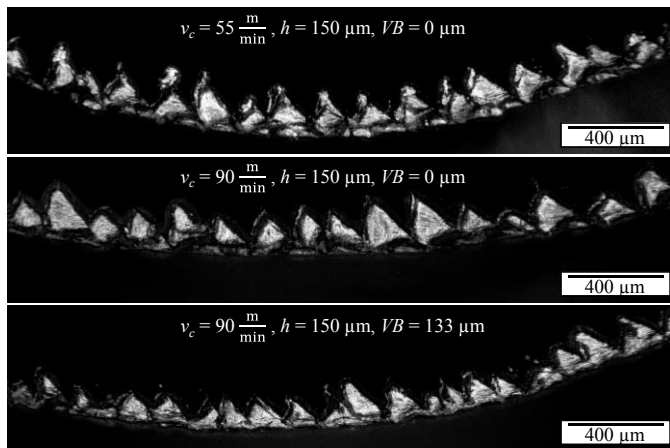


Fig. 5. Light microscopic images of the resulting segmented chips.

3.2. Signal processing

Raw sampled AE data $x[n] = x(nt_s)$ with sample time t_s are converted into time-frequency representation by discrete STFT, because transient signal portions during cutting process and time-dependent variables have to be analyzed in time-dependent frequency representation. Discrete STFT is calculated by

$$F_x^\gamma[m, k] = \sum_{n=0}^{N-1} x[n] \gamma_{mk}^*[n] \quad (1)$$

In this equation, a conjugate complex, time and frequency shifted analysis window is used:

$$\gamma_{mk}[n] = \gamma((n - m \Delta M) t_s) e^{-j2\pi kn/K} \quad (2)$$

The function $\gamma(t)$ is a Gaussian window of range $t \in [-2.5\sigma, 2.5\sigma]$ in this case, where $\sigma = 1.048\ \text{ms}$ represents the standard deviation of $\gamma(t)$. In order to transform the entire AE data, $\gamma(nt_s)$ is shifted in time for $m \cdot \Delta M$ sampled data points of sample time t_s , where $\Delta M \cdot t_s$ corresponds to the half of the window size. Consequently, each window is $\Delta t = 5.24\ \text{ms}$ wide and overlaps half of the neighbor windows. In equation (1), m is the discrete time index of STFT and the index k represents defined frequencies, up to maximum frequency index $K-1$. Both time and frequency data points are scaled equidistantly.

In order to further analyze occurring frequencies, the absolute STFT values $|F_x^\gamma[i, k]|$ of every time step $i \in [i_0, i_c)$ during orthogonal cutting and the whole frequency range are separated. Temporal averages are calculated for each frequency bin $k \in [0, K-1]$ by means of the appropriate absolute STFT values:

$$P_x^\gamma[k] = \frac{1}{i_c - i_0} \sum_{i=i_0}^{i_c-1} |F_x^\gamma[i, k]|^2 \quad (3)$$

Each squared absolute STFT value $|F_x^\gamma[i, k]|^2$ represents an estimation of the energy density at time i and frequency k . The temporal averages $P_x^\gamma[k]$ of those energy densities are combined in a frequency-dependent periodogram. Due to analysis by periodograms, signal noise energy is reduced and frequencies are emphasized, which have been detected during the entire cutting process.

3.3. Results and discussion

Although detailed frequency analysis is performed by means of the periodograms, time-frequency representations already show lots of process characteristics. Exemplarily, the time-frequency representation of orthogonal cutting with cutting speed of $v_c = 55\ \text{m/min}$ and new insert is illustrated in Fig. 6. Based on the grey-scale representation of the spectrogram in Fig. 6, machine operation can be located between $t = 1.46\ \text{s}$ and $t = 1.54\ \text{s}$ (bright stripe for the whole frequency range). This period corresponds to the time range of the realized orthogonal cutting test. At $f = 5\ \text{kHz}$, energy density values are very high during orthogonal cutting, therefore chip segmentation frequency is assumed to be around this frequency here. Additionally, steady-state interference signals of constant frequency can be seen, mostly before and after the cutting process.

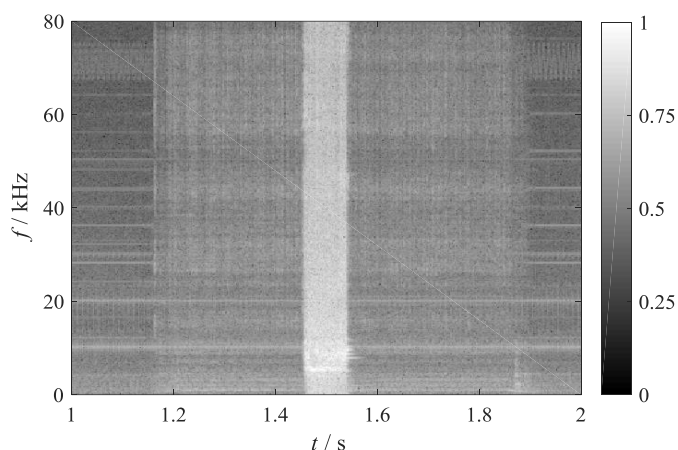


Fig. 6. Time-frequency representation of orthogonal cutting with cutting speed $v_c = 55$ m/min and new insert; logarithmic energy density in grey-scale values and normalized to maximum value (bright intensities correspond to high values).

Resulting periodograms, calculated as described in Section 3.2, are given in Fig. 7, in which the effect of different cutting speed is analyzed, and in Fig. 8, where the effect of tool wear is investigated.

In case of different cutting speed (Fig. 7), the frequency with maximum energy density for $v_c = 90$ m/min is significantly higher than the frequency for $v_c = 55$ m/min.

For orthogonal cutting with different inserts (Fig. 8), the frequencies of the calculated maximum energy densities are equal. Therefore, no relation between the condition of the insert and the maximum in periodogram can be stated. Possible reasons are the periodogram’s frequency resolution of $\Delta f \cong 190$ Hz and interference signals from the process, like the steady-state signals with constant frequency in Fig. 6. Instead of taking the frequency with maximum energy density, an analysis of harmonics leads to wear-dependent frequencies. In Fig. 8, two local maxima are labeled in the frequency range of the fifth harmonic of the maximum of the periodogram. The fundamental oscillations corresponding to these harmonics at $f = 44.06$ kHz and $f = 45.78$ kHz are $f = 8.81$ kHz for the new insert and $f = 9.16$ kHz for the worn insert.

Table 4 presents a comparison of the chip segmentation frequencies determined experimentally (by light microscopy) and those calculated by AE signals with respect to the relevant parameter configurations.

Table 4. Comparison of the chip segmentation frequencies determined experimentally (by light microscopy) and those calculated from AE signals during orthogonal cutting.

v_c	55 m/min	90 m/min	90 m/min
h	150 μm	150 μm	150 μm
VB	0 μm	0 μm	133 μm
$f_{cs, \text{exp}}$	5.45 kHz	8.38 kHz	9.66 kHz
$f_{cs, \text{AE}}$	5.15 kHz	8.81 kHz	9.16 kHz

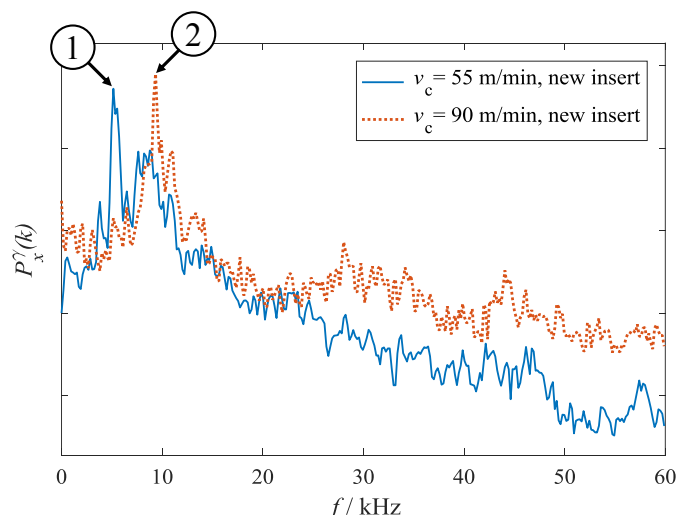


Fig. 7. Periodogram (logarithmically scaled) based on STFT of orthogonal cutting of Ti-6Al-4V with different cutting speed v_c .
1) $f = 5.15$ kHz, 2) $f = 9.346$ kHz.

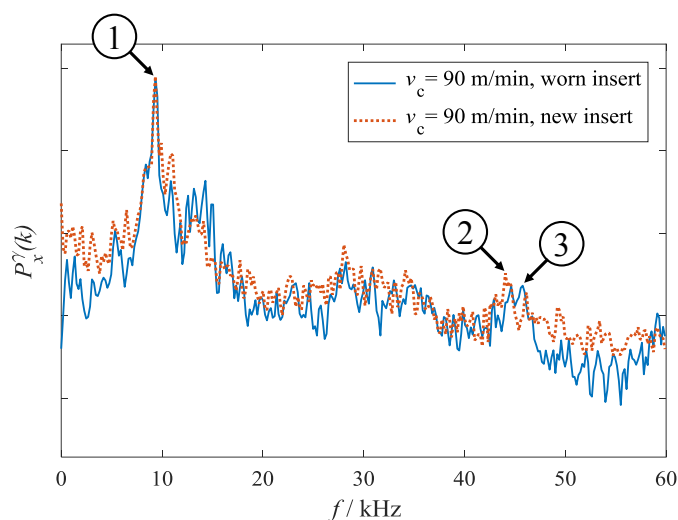


Fig. 8. Periodogram (logarithmically scaled) based on STFT of orthogonal cutting of Ti-6Al-4V with new and worn insert.
1) $f = 9.346$ kHz, 2) $f = 44.06$ kHz, 3) $f = 45.78$ kHz.

The experimental results obtained by light microscopy conform to the acoustic emission results. All respective frequencies are in the same frequency range and show similar tendencies. This tendencies suit the simulated effects and the simulation results of Section 2.

Small deviations in the frequency results of Table 4 occur, for example, due to varying chip segmentation frequency and frequency resolution of $\Delta f \cong 190$ Hz of the periodograms. Furthermore, frequencies measured by light microscopy strongly depend on the examined part of the chip.

As the frequencies have been determined in the same range and with similar tendencies, a measurable correlation between chip segmentation frequency and residual stress state can be stated. Consequently, the process can be monitored by AE and the component’s residual stress state can be controlled with the knowledge of the simulation results.

4. Conclusion

The possibility of assessing the component's residual stress state by means of the acoustically measured chip segmentation frequency was investigated for the orthogonal cutting of Ti-6Al-4V alloy. FEM simulations were undertaken in order to investigate the correlation between the cutting speed v_c , tool wear state, residual stress state and chip segmentation frequency f_{cs} . Furthermore, chip segmentation frequency could be measured by means of acoustic emission signals and subsequent signal processing in orthogonal cutting tests. The key findings of this work are:

- The chip segmentation has a direct impact on the residual stress depth distribution as well as on the temporal evolution of the cutting force F_c and chip segmentation frequency f_{cs} .
- A higher amount of induced surface compressive residual stresses along with a significant decrease in chip segmentation frequency f_{cs} can be stated for decreasing cutting speed v_c .
- A significant decrease of induced compressive residual stresses into the component's surface layer along with a slight increase of chip segmentation frequency f_{cs} can be stated for a growing tool wear state.
- Chip segmentation frequency during orthogonal cutting of Ti-6Al-4V can be monitored in-process using time-frequency analysis of acoustic emission signals.

Consequently, the acoustically measured chip segmentation frequency f_{cs} emerges as a process-characteristic variable with a high potential for assessing the component's residual stress state during machining of Ti-6Al-4V alloy. The hypothesis of compensating the negative effect of tool wear on the component's residual stress state by means of targeted adjustment of the process parameters can be derived and will be aimed in future work.

References

- [1] Zanger F. Segmentspannung, Werkzeugverschleiß, Randschichtzustand und Bauteileigenschaften: Numerische Analysen zur Optimierung des Zerspanungsprozesses am Beispiel von Ti-6Al-4V. Dissertation, 2012; Karlsruhe Institute of Technology.
- [2] Childs T. Adiabatic Shearing in Metal Machining. The International Academy for Production Engineering, Laperrière L., Reinhart G. (eds) CIRP Encyclopedia of Production Engineering. Springer, Berlin, Heidelberg, 2014.
- [3] Nguyen V., Fernandez-Zelaia P., Melkote S. N. PVDF sensor based characterization of chip segmentation in cutting of Ti-6Al-4V alloy. CIRP annals – Manufacturing Technology, 2017; 66:73-76.
- [4] Schulze V., Zanger F. Development of a simulation model to investigate tool wear in Ti-6Al-4V alloy machining. Advanced Materials Research, 2011; 223:535-544.
- [5] Johnson G.R., Cook W.H. A constitutive model and data for metals subjected to large strains, high strain rates and high temperatures. Proceedings of the 7th International Symposium on Ballistic, the Hague, Netherlands, 1983; 541-547.
- [6] Recht R.F. Catastrophic Thermoplastic Shear. ASME Transactions Journal of Applied Mechanics, 1964; 86:189-193.
- [7] Sun J., Guo Y. Material flow stress and failure in multiscale machining titanium alloy Ti-6Al-4V. International Journal of Advanced Manufacturing Technology, 2009; 41:651-659.
- [8] Schulze V., Zanger F. Numerical Analysis of the Influence of Johnson-Cook-Material Parameters on the Surface Integrity of Ti-6Al-4V. Conference on Surface Integrity, Procedia Engineering, 2011; 19:306-311.
- [9] Chen L., El-Wardany T.I., Harris W.C. Modeling the Effects of Flank Wear Land and Chip Formation on Residual Stresses. CIRP Annals – Manufacturing Technology, 2004; 53(1):95-98.
- [10] Sun S., Brandt M., Dargusch M.S. Characteristics of cutting forces and chip formation in machining of titanium alloys. International Journal of Machine Tools & Manufacture, 2009; 49:561-568.
- [11] Barry J., Byrne G., Lennon D. Observations on chip formation and acoustic emission in machining Ti-6Al-4V alloy. International Journal of Machine Tools & Manufacture, 2001; 41:1055-1070.
- [12] Maradei C., Piotrkowski R., Serrano E., Ruzzante J. Acoustic emission signal analysis in machining processes using wavelet packets. Latin American applied research, 2003; 33(4):443-448.
- [13] Gopikrishnan A., Kanthababu M., Nizamudheen A.K. Acoustic Emission Signal Analysis for Tool Condition Monitoring in Microturning of Titanium Alloy. Advanced Materials Research, 2014; 984-985:31-36.
- [14] Menon A. K., Boutaghou Z.-E. Time-frequency analysis of tribological systems – Part I: implementation and interpretation. Tribology International, 1998; 31(9):501-510.